TECHNICAL ARTICLE

Monitoring of CoS_2 reactions using high-temperature XRD coupled with gas chromatography (GC)

Mark A. Rodriguez,[a] Eric N. Coker, James J. M. Griego, Curtis D. Mowry, Adam S. Pimentel, and Travis M. Anderson
Sandia National Laboratories, Albuquerque, New Mexico 87185-1411

(Received 19 February 2016; accepted 24 March 2016)

High-temperature X-ray diffraction with concurrent gas chromatography (GC) was used to study cobalt disulfide cathode pellets disassembled from thermal batteries. When CoS_2 cathode materials were analyzed in an air environment, oxidation of the K(Br, Cl) salt phase in the cathode led to the formation of K_2SO_4 that subsequently reacted with the pyrite-type CoS_2 phase leading to cathode decomposition between ~260 and 450 °C. Independent thermal analysis experiments, i.e. simultaneous thermogravimetric analysis/differential scanning calorimetry/mass spectrometry (MS), augmented the diffraction results and support the overall picture of CoS_2 decomposition. Both gas analysis measurements (i.e. GC and MS) from the independent experiments confirmed the formation of SO_2 off-gas species during breakdown of the CoS_2. In contrast, characterization of the same cathode material under inert conditions showed the presence of CoS_2 throughout the entire temperature range of analysis. © *2016 International Centre for Diffraction Data.* [doi:10.1017/S0885715616000166]

Key words: CoS_2, HTXRD/GC, TGA/DSC/MS, cobalt sulfide, thermal batteries

I. INTRODUCTION

Transition metal sulfide compounds such as CoS_2 can be employed for energy storage purposes such as anodes for Li-ion batteries (Goriparti *et al.*, 2014), as materials for supercapacitor applications (Bao *et al.*, 2008), and cathodes for thermal batteries (Butler *et al.*, 2004). The cobalt sulfide phase diagram, as documented by Mrowec *et al.* (1998), contains many compounds including Co_4S_3, $Co_{1-y}S$, Co_9S_8, Co_3S_4, and CoS_2. The different compositions are often a result of different synthesis conditions such as temperature and atmosphere. Additionally, oxidation of cobalt sulfide phases can occur depending on the pO_2 present during heat treatment.

We have employed high-temperature X-ray diffraction (HTXRD) along with concurrent gas chromatography (GC) to monitor and document the behavior of CoS_2 thermal battery cathode materials during heat treatment. There has been very little work published on research diagnostics for *in situ* gas analysis with simultaneous diffraction characterization. Some early work by Fawcett (1987) demonstrated the means of performing *in situ* XRD with simultaneous mass spectrometry (MS) and differential scanning calorimetry (DSC). Our method is similar in design, but employs a different gas analysis method (GC) for diagnosis of the gaseous species. There are benefits and drawbacks to selection of GC vs. MS. The main differences are that while MS can be more definitive in terms of a clear identification of a gaseous species, GC performs better for purposes of quantification of gas presence and can more easily separate gas components via retention time. Another publication (Coker *et al.*, 2011) reports the use of GC with HTXRD for detecting the presence of CO gas evolved during a thermochemical cycle. This early work by Coker *et al.* (2011) details the first use of GC concurrent with HTXRD. The results presented below expand upon the use of HTXRD/GC and document its use as applied to CoS_2 cathode materials. Our HTXRD/GC analysis has been augmented by the addition of simultaneous thermal analysis (STA) where both thermogravimetric analysis (TGA) and DSC are collected simultaneously. This method also employed the use of MS for analysis of the off-gas species. Therefore, this second independent experiment has been referred to as TGA/DSC/MS as they are all collected together in a single comparable dataset.

II. EXPERIMENTAL

Specimens of a cathode were taken from an existing battery build and were kept under vacuum until analysis. The cathode consisted of CoS_2 powder (Cerac, 99.4% purity) mixed with a solid-solution electrolyte (KBr, Cl) and a trace addition of Li_2O. Cathode materials were split, so that one portion of the cathode had HTXRD/GC analysis performed, while a second piece of the cathode was analyzed using comparative thermal analysis via TGA/DSC/MS. In this way, two comparative datasets could be tabulated with a combined total of five analytical characterization techniques. Sample powders were ground to a fine powder prior to analysis.

A. HTXRD/GC

Figure 1 shows a picture of the X-ray diffractometer equipped with the furnace chamber. The HTXRD system is a Scintag PAD X powder X-ray diffractometer employing a sealed tube Cu$K\alpha$ X-ray source, an incident beam mirror

[a] Author to whom correspondence should be addressed. Electronic mail: marodri@sandia.gov

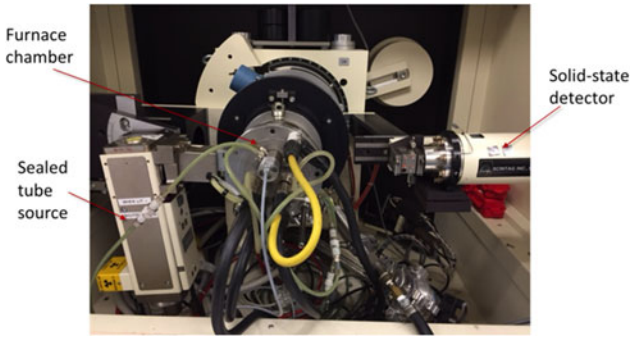

Figure 1. (Color online) HTXRD system configured with hot stage (furnace chamber).

optic, fixed receiving slits and a Peltier-cooled germanium solid-state detector. The ancillary hot-stage was a Buehler HTK 2400 furnace with a Pt/Rh heating strip and surround heater. The temperature of the hot-stage furnace was calibrated via thermal expansion of known standard materials (e.g. alumina) while being run under similar conditions as the samples. Cathode powders were ground under methanol and coated onto the alumina substrates for loading onto the heating strip. Figure 2 shows the setup of the gas handling system for flowing either air or inert (N_2) gas. Mass flow controllers were plumbed between the gas cylinders and the input to the furnace chamber. This was for experiments which required gas mixing; these were not employed in our experiments because the air (Matheson Ultra Zero) and N_2 (Matheson UHP) gases were used directly from the as-received cylinders. One can also see an oxygen getter on the equipment rack. While this was unused in the current experimental design, it could be employed if very low pO_2 levels are desired (i.e. <1 ppm O_2). The other two items of equipment in the gas handling system shown in Figure 2 were the micro-GC (μ-GC) (Agilent CP-4900) and an oxygen meter (Ameteck CG1000). These were plumbed in parallel into the vent line from the furnace chamber. The μ-GC has two columns; Molecular Sieve 5A (MSA) and PoraPLOT U (PPU), and is referred to as a μ-GC, due to its compact nature and small footprint. The μ-GC was configured to sample gas in ~2 min increments. This worked well to monitor the gas conditions during the HTXRD measurements, which occurred in an increment of 4.5 min per scan at a given hold temperature. XRD scan parameters were as follows: angular range = 20–54°2θ, step-size = 0.05°2θ, count time = 0.4 s, heating rate between scans = 50 °C min^{-1}, temperature increment between scans = 25 °C. Using these scan parameters for HTXRD data collection, the effective heating rate mimics a ~5 °C min^{-1} heating rate from the start of the experiment up to the maximum temperature of 550 °C.

B. TGA/DSC/MS

Figure 3 shows the setup for the STA instrumentation. The system is a Netzsch STA 409-CD TGA/DSC system. TGA allows for determination of weight gain or loss with heating, while DSC indicates the existence of an endothermic or exothermic reaction at a given temperature. Cathode fragments were loaded into alumina crucibles for analysis. The system was also equipped with a Hiden Analytical HPR-20 mass spectrometer (MS) to diagnose the gaseous species that were generated during heating. Employing MS for characterization of off-gas species during STA is relatively common. For example, see Trionfetti *et al.* (2006) and Choi *et al.* (2011). The MS instrument (as shown in Figure 3) drew a constant stream of gas from the vent line of the TGA/DSC system. The thermal analysis experiments and HTXRD measurements were performed independently, but were matched in time and heating rate to be comparable between the two datasets. The heating rate employed for the thermal analysis was 5 °C min^{-1} and the maximum temperature 600 °C. Comparison of results from TGA/DSC/MS with those of HTXRD/GC shed light on the breakdown of CoS_2 during heat treatment in an oxidizing condition (air) as will be documented below. A control experiment under inert conditions was also run. This was performed under N_2 gas for HTXRD/GC and under argon gas for the TGA/DSC/MS experiment.

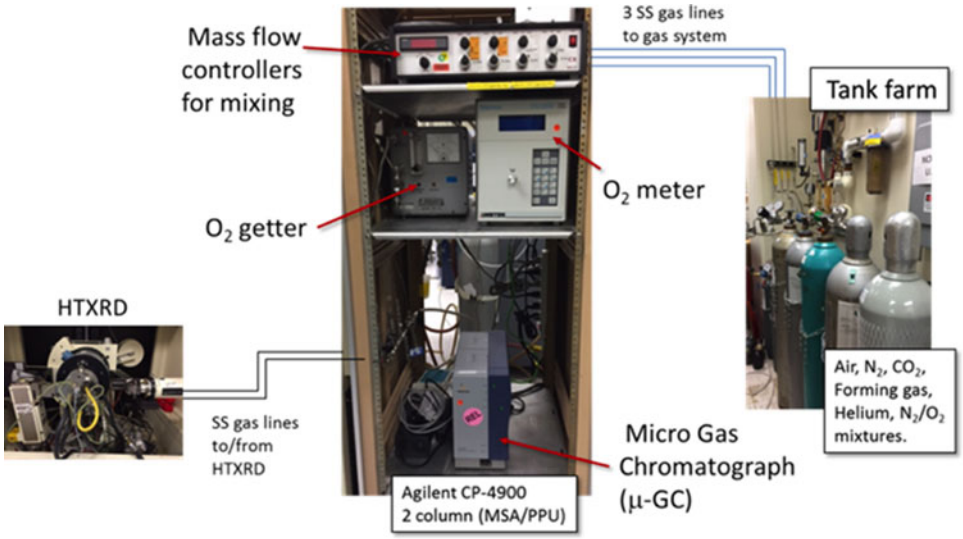

Figure 2. (Color online) Configuration of gas handling system showing gas cylinders, mass flow controllers, O_2 getter, O_2 meter, and Agilent CP-4900 μ-GC.

https://doi.org/10.1017/S0885715616000166 Published online by Cambridge University Press

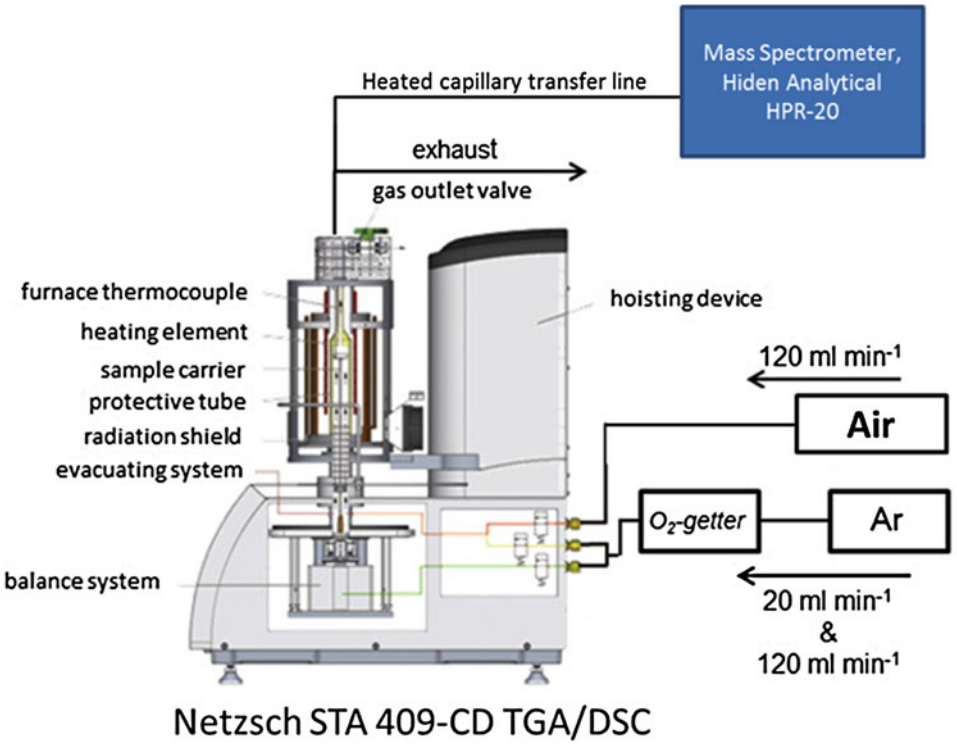

Figure 3. (Color online) Schematic diagram of the STA system as configured with MS.

III. RESULTS AND DISCUSSION

A. CoS_2 analysis under air atmosphere

Heating of the CoS_2 powder within the HTXRD reaction chamber with simultaneous diffraction measurement yields a dynamic picture of multiple reactions occurring over the 25–550 °C temperature range. Figure 4 shows the results for the CoS_2 cathode sample run under flowing air. The plot shows data as $°2\theta$ on the *x*-axis, temperature (°C) on the *y*-axis, and a color scale for intensity where low counts are black, high counts are white, and intermediate counts vary from red to orange to yellow. Figure 4 shows some important observations. First, the as-received cathode material is confirmed to be dominated by two phases, CoS_2, PDF 04-003-1962 (ICDD, 2015), with a Pyrite-type structure (as shown by several peaks for this phase), and a salt phase labeled here as K(Br,Cl), PDF 01-081-9940 (ICDD, 2015). The K(Br,Cl) phase is a salt phase similar to KBr but also contains a fraction of Cl substituted for Br in the salt lattice. This creates a solid-solution salt phase, which likely serves to reduce the melting point of the salt. One can see that these two initial phases decompose (*vida infra*) between 300 and 400 °C along with the formation of other phases such as K_2SO_4, PDF 04-017-4456 (ICDD, 2015), and ultimately Co_3O_4, PDF 04-005-4386 (ICDD, 2015).

Concurrent GC analysis was collected during this experiment. The results are shown in Figure 5. This color contour graph plots retention time on the *x*-axis, temperature on the *y*-axis and intensity as a color scale where low counts are black, high counts are white, and intermediate counts vary from red to orange to yellow. The results only show a small portion of the ~2 min μ-GC scan, but the plot illustrates the

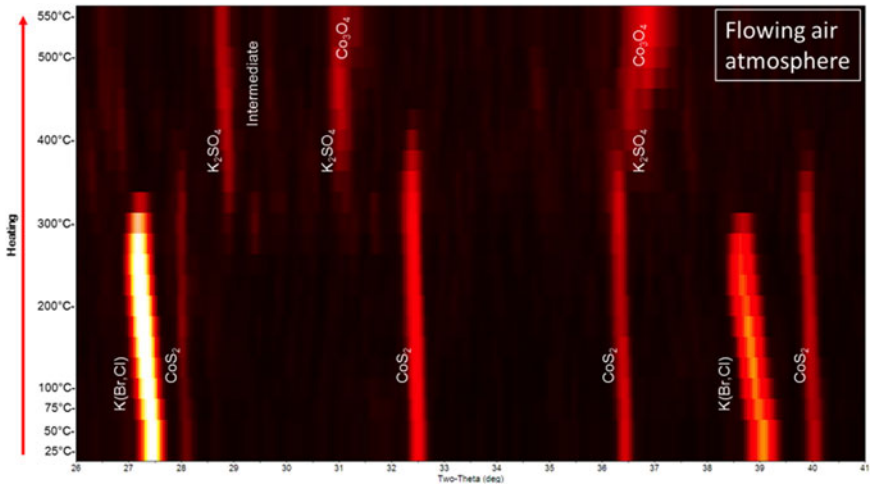

Figure 4. (Color online) HTXRD results for CoS_2 cathode under the flowing air atmosphere. See the text for details.

https://doi.org/10.1017/S0885715616000166 Published online by Cambridge University Press

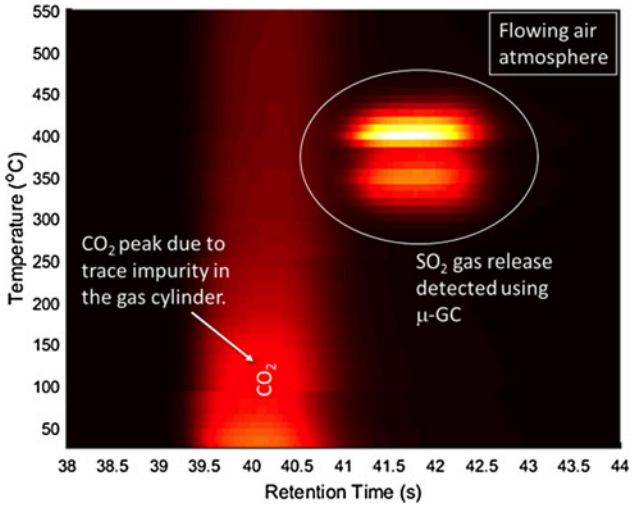

Figure 5. (Color online) μ-GC results for the CoS_2 cathode heated in flowing air showing formation of SO_2 gas between 300 and 450 °C. A small trace of impurity CO_2 gas was also detected and was determined to be experimental artifact.

dominant activity in terms of gaseous species. The graph clearly shows a major gas release between 300 and 450 °C at the ~42 s retention time. This signal was confirmed to be due to SO_2 gas as determined by calibration standards run separately on the PPU column. The SO_2 gas appears to come off at two distinct temperatures, 350 and 400 °C with the majority gas loss occurring at the 400 °C temperature. Clearly this temperature range looks to be where most of the chemical activity occurs. Additionally, there is signal at about 40 s retention time and it persists over the entire temperature range. The intensity of this additional peak appears to be stronger at room temperature with a gradual decay over time. This signal was confirmed to be from CO_2 gas and its presence was determined to be from both the ambient air during sealing of the reaction chamber (furnace) as well as a small impurity of CO_2 in the dry air cylinder. For this experiment, the small presence of CO_2 can be ignored as it is unaffiliated with the cathode behavior.

Thermal analysis revealed a great deal of information regarding the changes detected in the HTXRD/GC experiment. Figure 6 shows the TGA/DSC results when CoS_2 cathode material was run in flowing air. The graph shows two datasets, the plot in red (top) is from the DSC and the black (bottom) is from TGA. The *x*-axis plots temperature. The right side of the graph plots heat flow for the DSC data where exothermic is shown as a negative value (default for Netzsch systems). The *y*-axis on the left is for TGA and shows % weight gain or loss. What is immediately obvious from this graph is that a major reaction occurs at ~265 °C as shown in the exotherm in the DSC. This is also concurrent with a weight increase as seen in the TGA trace. The XRD data indicate that K_2SO_4 is forming above this temperature. The exothermic reaction is telling because it suggests oxidation of the K(Br,Cl) salt phase to form potassium sulfate. This exothermic reaction is in stark contrast to the expected behavior, which would be melting of the salt phase to form a liquid electrolyte. This first oxidizing reaction sets the stage for other reactions.

The STA data in Figure 6 also show other activity at higher temperatures. The mass gain predominantly due to K_2SO_4 formation achieves a maximum of ~106% of the initial sample weight at ~350 °C. This is followed by a significant mass loss, with the maximum rate of weight loss (steepest slope in the TGA data) occurring just above 400 °C. This is consistent with the off-gassing of SO_2 as observed in the μ-GC data in Figure 5. Additional support for off-gassing of SO_2 was obtained from the MS data collected during the TGA/DSC measurement. Figure 7 shows the results of the MS analysis. It shows a broad and somewhat asymmetric peak for a gaseous species with mass/charge ratio of ~64 amu (SO_2). The peak in Figure 7 grows more gradually at low temperatures, beginning at ~265 °C, the same temperature as the onset of K_2SO_4 formation as documented via HTXRD in Figure 4. The maximum SO_2 gas release for the MS data in Figure 7 looks to occur at ~400 °C, and drops off quickly above 500 °C. When comparing the MS data in Figure 7 with that of the μ-GC results in Figure 5 one can see that the μ-GC results show two distinct release maxima (~350 and 400 °C), while the plot for the MS shows essentially one asymmetrically shaped peak without distinctly separated maxima. The explanation for this discrepancy may be related to the different heating schedules in the two experiments. On average, the heating rate was ~5 °C min^{-1} in both experiments. However, the TGA/DSC/MS used an actual 5 °C min^{-1} heating rate. In contrast, the HTXRD/GC used a series of step and hold

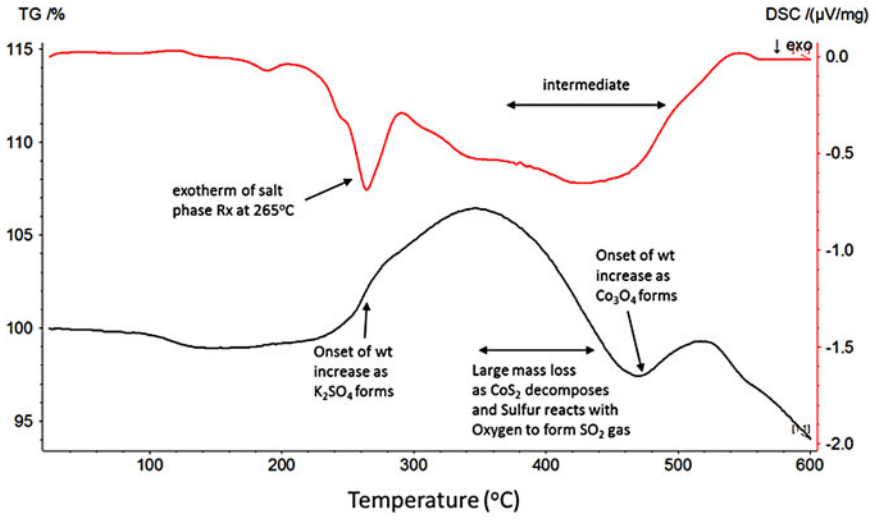

Figure 6. (Color online) Thermal analysis results for the CoS_2 cathode processed in an air atmosphere. See the text for details.

https://doi.org/10.1017/S0885715616000166 Published online by Cambridge University Press

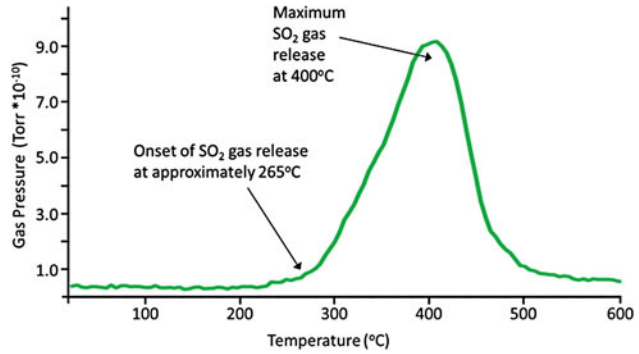

Figure 7. (Color online) MS data for the CoS_2 cathode processed in an air atmosphere.

temperatures. The constant heating rate of the TGA/DSC/MS measurement likely results in an averaging effect for the thermal behavior, while the step and hold measurement for HTXRD/GC likely leads to a more discrete dataset. Looking again at the MS data in Figure 7, one could imagine a second smaller peak centered at ~350 °C that is superimposed upon the larger peak centered at ~400 °C, where the second peak accounts for the asymmetric skew in the overall profile. Hence, the data for the two gas analysis techniques can be reconciled. The XRD results from Figure 4 show that shortly after the formation of K_2SO_4 at approximately 380 °C one observes the formation of what shall be referred to as an intermediate compound. The exact composition of this phase remains uncertain; however, possible candidate phases include $K_2Co_2(SO_4)_3$, PDF 00-020-0873 (ICDD, 2015), and K_9CoS_7, PDF 04-010-8100 (ICDD, 2015). The compound is coined an intermediate because it serves as a medium between the pure sulfide CoS_2 and the fully oxidized Co_3O_4 that forms at higher temperatures. The intermediate phase appears to be a decomposition product from the reaction of CoS_2 with K_2SO_4. This reaction results in the release of SO_2 gas as confirmed by both μ-GC and MS. The competing reactions of K_2SO_4 formation and breakdown of CoS_2 result in the maximum for TGA weight gain at ~350 °C (see TGA trace in Figure 6). Between 350 and 400 °C one observes a fast decay of the CoS_2 peaks in the HTXRD data, as seen in Figure 4, consistent with the formation of the intermediate phase. Finally, the XRD data (Figure 4) indicate conversion of the intermediate to Co_3O_4 beginning at ~450 °C and becoming dominant

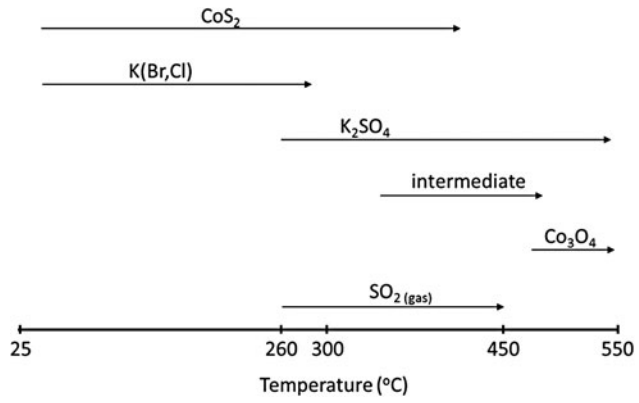

Figure 8. The reaction sequence for breakdown of the CoS_2 cathode materials processed in air.

by 550 °C. The TGA data in Figure 6 actually show a change to a weight gain starting at ~460°C, which continues to increase in quantity up to ~520 °C. This weight gain is associated with the formation of Co_3O_4 once the CoS_2 and intermediate phases have converted the reactive sulfur to SO_2 gas. K_2SO_4 continues to persist up to 550 °C in the HTXRD data. Hence, the K_2SO_4 may serve as a catalyst for the breakdown of CoS_2 to ultimately form the oxide Co_3O_4.

To summarize, the reaction sequence can be shown using the schematic diagram given in Figure 8. This figure illustrates graphically the reaction sequence that occurs when heating the CoS_2 cathode in the presence of an air atmosphere along with the presence of a K(Br,Cl) salt. The clear demarcation of this reaction sequence occurs with the conversion of the salt to K_2SO_4. It appears that K_2SO_4 formation is a critical first step in the decomposition process, since K_2SO_4 looks to be a critical constituent in the cascading reaction of CoS_2 to form the intermediate compound, which ultimately decomposes to the full oxide Co_3O_4. The presence of SO_2 gas is detected at the onset of the K_2SO_4 formation at ~260 °C, likely due to the consumption of a fraction of the CoS_2 cathode. The exothermic nature of this reaction is demonstrative of this oxidizing condition. With the presence of K_2SO_4, further reaction to form the intermediate phase progresses with significant loss of SO_2 gas between 260 and 450 °C with a maximum SO_2 loss occurring at ~400 °C, which also corresponds to the highest rate of weight loss in the sample after an initial weight gain during K_2SO_4 formation. The final conversion of the intermediate phase to Co_3O_4 is demonstrated by a small weight gain above ~500 °C and the cessation of SO_2 gas loss.

B. CoS_2 analysis under inert atmosphere

It is worth documenting as well the behavior of a cell processed under inert conditions so that a comparison can be made in regard to proper and expected performance of the cathode. Figure 9 shows the HTXRD results for the same CoS_2 cathode material heated under flowing N_2 gas (pO_2 of between 2 and 10 ppm). The contour plot shows identical results to that of Figure 4 in the lower temperature regions (below 250 °C) with the same CoS_2 and K(Br, Cl) phases detected. However, what is markedly different in Figure 9 is that the CoS_2 remains present over the entire temperature range without breakdown, as indicated by the continuous presence of the CoS_2 peaks traversing the entire temperature range. This is desirable in the sense that the battery will perform in the expected manner if the CoS_2 phase persists to operating temperatures. What is also very important is the observation that the K(Br, Cl) peaks persist well above 300 °C. They do appear to decrease in intensity as the temperature is increased above 300 °C, but the salt peaks are definitely more significant above 300 °C under N_2 atmosphere, as compared with air as seen in Figure 4. This suggests a different behavior of the salt phase when under inert conditions.

Figure 10 shows the μ-GC data collected during the HTXRD experiment under inert conditions. This graph shows no evidence of SO_2 gas evolution at any temperature up to 550 °C, but only shows the CO_2 gas artifact, similar to that in the air analysis. This is additional supporting evidence of a stable CoS_2 phase with temperature under these inert gas conditions. Thermal analysis data collected on the same CoS_2 cathode sample (in this case run under argon as the inert gas)

https://doi.org/10.1017/S0885715616000166 Published online by Cambridge University Press

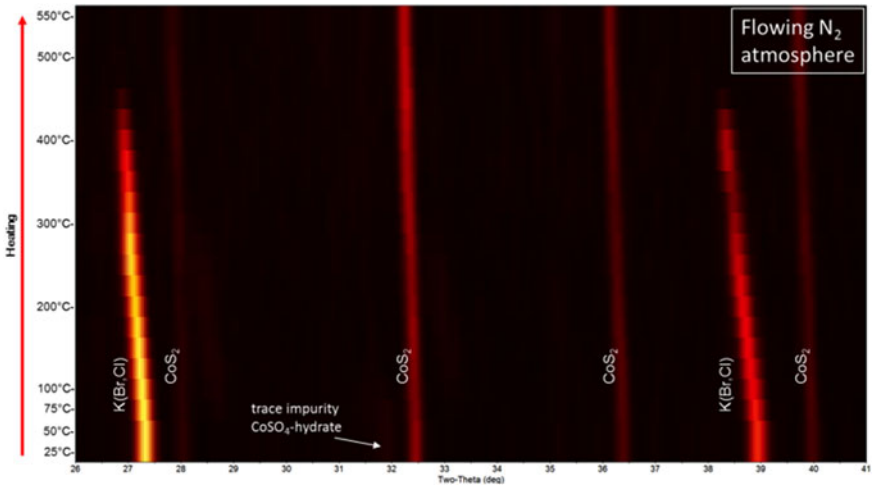

Figure 9. (Color online) HTXRD results for the CoS_2 cathode material under flowing N_2 gas. See the text for details.

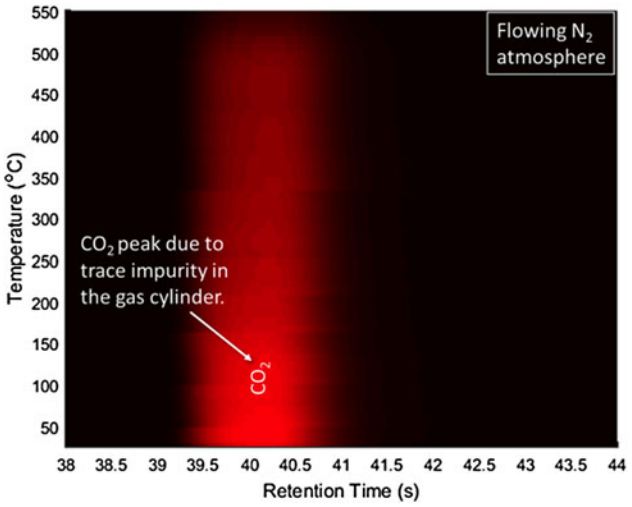

Figure 10. (Color online) μ-GC results for the CoS_2 cathode material under flowing N_2 gas as collected during the HTXRD run (Figure 9).

showed very different behavior as compared to the air analysis. Figure 11 shows the TGA/DSC traces for the inert gas run. Here we see a very important observation of an endothermic peak at ~300 °C. This observation indicates a melting transition and can be associated with the melting of the electrolyte [nominally K(Br, Cl) salt] phase. The low temperature of melting is a bit of a surprise in that the melting points of KBr and KCl are 734 and 770 °C, respectively. Certainly, a solid solution of K(Br,Cl) will melt at a lower temperature due to melting point depression of the solid-solution phase, though a drop of almost 400 °C is unlikely. However, when one considers the nominal preparation of the cathode powder, our analysis suggests that the Li addition in the cathode powder (initially as Li_2O) has aided in the reduced temperature of melting for the electrolyte. Indeed, Li-containing electrolytes are known to possess melting points about 300 °C. Clearly the salt must melt prior to the operating temperature of the designed battery, so it follows that the salt should melt somewhere between 300 and 400 °C and this is confirmed in the STA and HTXRD results.

It is also notable that there are changes in the TGA/DSC curves between room temperature and ~140 °C for the sample heated under inert gas. There is a clear weight loss, which occurs at ~100 °C and an endothermic peak at ~120 °C. These thermal events can be traced to the dehydration of a $CoSO_4$-hydrate phase, which was observed in small quantities in the sample prior to heating. These deviations look significant in Figure 11, but if one compares the magnitudes of the *y*-axes scales to that of Figure 6 for the air-processed sample one can see that Figure 11 has a much smaller scale range for both the TGA and DSC. In fact, if one looks at the data

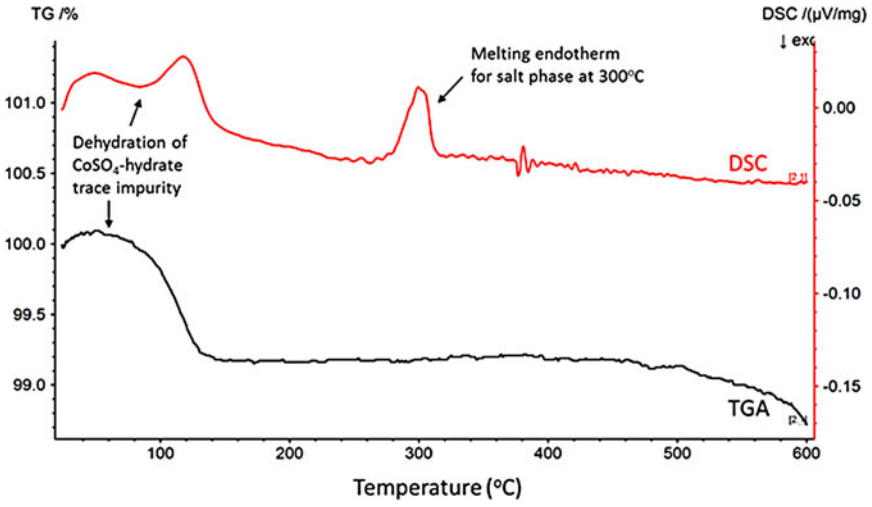

Figure 11. (Color online) Thermal analysis results for the CoS_2 cathode material processed under inert (Ar gas) atmosphere. See the text for details.

https://doi.org/10.1017/S0885715616000166 Published online by Cambridge University Press

in the range of room temperature to ~140 °C in Figure 6, one can see similar behavior of a small weight loss in the TGA and endothermic peaks in the DSC trace. However, they are weak and suppressed to the background in Figure 6 due to the magnitude of other thermal events. So it appears that a small fraction of CoS_2 is reacted to form the $CoSO_4$-hydrate, even prior to heating, and it occurs in both samples. What also appears clear is that this small amount of impurity does not look to change the outcome of the experiments presented here.

No MS data are presented here for the thermal analysis experiment shown in Figure 11 as there was no detection of SO_2 gas from the sample during the TGA/DSC/MS experiment. This was consistent with the results of the μ-GC experiment run concurrent with HTXRD as shown in Figure 10. A small quantity of water was detected by MS during the early portions of the run, corroborating the dehydration shown in Figure 11.

IV. CONCLUSIONS

We have successfully integrated the use of GC with concurrent HTXRD analysis for characterization of CoS_2-based cathodes used in thermal batteries. The coupling of these two methods, HTXRD/GC with TGA/DSC/MS serves as a powerful set of diagnostics for characterizing chemical reactions *in situ* where there is the possibility of gas evolution during the reaction process. When CoS_2 cathode materials were analyzed in an air environment, oxidation of the salt phase in the cathode led to the formation of K_2SO_4 which subsequently reacted with CoS_2, leading to the decomposition of the CoS_2 phase. Independent thermal analysis experiments augment the HTXRD results and support the overall picture of CoS_2 decomposition. Coupling of these two techniques HTXRD/GC and TGA/DSC/MS has proven effective for identification of the chemical reactions responsible for CoS_2 decomposition in air, yielding a highly detailed picture of the sequence of reactions that occur, temperatures at which these reactions occur, and the impact of atmosphere in the degradation process. The oxidation behavior of CoS_2 will enable a clearer understanding of the decreased performance of thermal batteries exposed to air atmosphere during use. The exotherm at 260°C and evolution of SO_2 gas can serve as indicators of oxygen exposure and may therefore function as a predictive means of CoS_2 cathode degradation in thermal batteries. Control experiments performed under inert conditions verified the stability of the CoS_2 phase up to 550 °C without significant reaction or decomposition of this pyrite-type sulfide compound.

ACKNOWLEDGEMENTS

The authors would like to thank Christine White for CoS_2 cathode sample preparation and Marshall Reviere for his assistance with HTXRD/GC data collection experiments. Sandia is a multiprogram laboratory managed and operated by Sandia Corporation, a wholly owned subsidiary of Lockheed Martin Corporation, for the United States Department of Energy's National Nuclear Security Administration under contract DE-AC04-94AL85000.

Bao, S-J., Li, C. M., Guo, C-X., and Qiao, Y. (**2008**). "Biomolecule-assisted synthesis of cobalt sulfide nanowires for application in supercapacitors," J. Power Sources **180**, 676–681.

Butler, P., Wagner, C., Guidotti, R., and Francis, I. (**2004**). "Long-life, multi-tap thermal battery development," J. Power Sources **136**, 240–245.

Choi, D., Xiao, J., Joon Choi, Y., Hardy, J. S., Vijayakumar, M., Bhuvaneswari, M. S., Liu, J., Xu, W., Wang, W., Yang, Z., Graff, G. L., and Zhang, J-G. (**2011**). "Thermal stability and phase transformation of electrochemically charged/discharged $LiMnPO_4$ cathode for Li-ion batteries," Energy Environ. Sci. **4**, 4560–4566.

Coker, E. N., Ambrosini, A., Rodriguez, M. A., and Miller, J. E. (**2011**). "Ferrite-YSZ composites for solar thermochemical production of synthetic fuels: *in operando* characterization of CO_2 reduction," J. Mater. Chem. **21**, 10767–10776.

Fawcett, T. (**1987**). "Greater than the sum of its parts – a new instrument," Chemtech **17**, 564–569.

Goriparti, S., Miele, E., De Angelis, F., Di Fabrizio, E., Proietti Zaccaria, R., and Capiglia, C. (**2014**). "Review on recent progress of nanostructured anode materials for Li-ion batteries," J. Power Sources **257**, 421–443.

ICDD (**2015**). PDF-4+ 2015 (Database), edited by Dr. Soorya Kabekkodu, International Centre for Diffraction Data, Newtown Square, PA, USA.

Mrowec, S., Danielewski, M., and Wojtowicz, A. (**1998**). "Sulphidation of cobalt at high temperatures," J. Mater. Sci. **22**, 2617–2628.

Trionfetti, C., Babich, I. V., Seshan, K., and Lefferts, L. (**2006**). "Formation of high surface area Li/MgO-Efficient catalyst for the oxidative dehydrogenation/cracking of propane," Appl. Catal. A: Gen. **310**, 105–113.

https://doi.org/10.1017/S0885715616000166 Published online by Cambridge University Press